ANNUAL REVIEWS

Annual Review of Earth and Planetary Sciences

Evolution of Atmospheric O_2 Through the Phanerozoic, Revisited

Benjamin J.W. Mills,[1] Alexander J. Krause,[2] Ian Jarvis,[3] and Bradley D. Cramer[4]

[1]School of Earth and Environment, University of Leeds, Leeds, United Kingdom; email: b.mills@leeds.ac.uk

[2]Department of Earth Sciences, University College London, London, United Kingdom; email: a.krause@ucl.ac.uk

[3]Department of Geography, Geology, and the Environment, Kingston University London, Kingston upon Thames, United Kingdom

[4]Department of Earth and Environmental Sciences, University of Iowa, Iowa City, Iowa, USA

Annu. Rev. Earth Planet. Sci. 2023. 51:253–76

First published as a Review in Advance on January 6, 2023

The *Annual Review of Earth and Planetary Sciences* is online at earth.annualreviews.org

https://doi.org/10.1146/annurev-earth-032320-095425

Keywords

oxygen, Phanerozoic, carbon cycle, geochemistry, evolution, animals

Abstract

An oxygen-rich atmosphere is essential for complex animals. The early Earth had an anoxic atmosphere, and understanding the rise and maintenance of high O_2 levels is critical for investigating what drove our own evolution and for assessing the likely habitability of exoplanets. A growing number of techniques aim to reproduce changes in O_2 levels over the Phanerozoic Eon (the past 539 million years). We assess these methods and attempt to draw the reliable techniques together to form a consensus Phanerozoic O_2 curve. We conclude that O_2 probably made up around 5–10% of the atmosphere during the Cambrian and rose in pulses to ~15–20% in the Devonian, reaching a further peak of greater than 25% in the Permo-Carboniferous before declining toward the present day. Evolutionary radiations in the Cambrian and Ordovician appear consistent with an oxygen driver, and the Devonian "Age of the Fishes" coincides with oxygen rising above 15% atm.

- An oxygen-rich atmosphere is essential for complex animals such as humans.
- We review the methods for reconstructing past variation in oxygen levels over the past 539 million years (the Phanerozoic Eon).

- We produce a consensus plot of the most likely evolution of atmospheric oxygen levels.
- Evolutionary radiations in the Cambrian, Ordovician, and Devonian periods may be linked to rises in oxygen concentration.

1. THE IMPORTANCE OF OXYGEN

All free-living animals and plants require molecular oxygen (O_2) to perform aerobic respiration. This places atmospheric oxygen at the heart of discussions about what has driven the evolution of Earth's biosphere and, more generally, about the potential for intelligence to have developed elsewhere in the universe. The early Earth was devoid of oxygen, but levels in the atmosphere and oceans have risen over time (Farquhar et al. 2000, Lyons et al. 2014). The first animals lived in the ocean and evolved in the Ediacaran period (Wood et al. 2019), about 570 million years ago (Ma), indicating that marine oxygen levels were sufficient to support their metabolisms by this time. During the following Cambrian period (538.8–486.9 Ma), life radiated explosively (Erwin et al. 2011), establishing almost all of the modern phyla (the highest subdivision of the kingdom of animals). The principal drivers of the Ediacaran and Cambrian radiations are still debated, but certainly the O_2 metabolic thresholds must have been crossed at some point prior to these evolutionary events (Sperling et al. 2013, Wood et al. 2019). Pulses of rapid animal evolution and extinction continued throughout the Phanerozoic, and the mass extinction events in the Late Ordovician (~445 Ma), Permian–Triassic (~252 Ma), and Triassic–Jurassic (~200 Ma) are convincingly linked to expansions of marine anoxia (waters lacking oxygen) (Wignall & Twitchett 1996, Ahm et al. 2017, He et al. 2020). However, the overall interplay between the volume of oxygenated water and animal evolution over the Phanerozoic remains uncertain—largely because the concentration of oxygen in the atmosphere and oceans over geological time is not well known.

When considering the evolution of intelligence, a useful question is, "What is the earliest point in Earth history during which humans could have survived on Earth's surface?" The answer would give an indication of what kind of biosphere was needed on our planet to support intelligence as we know it, and therefore what evolutionary advances might be needed for intelligence to arise on an exoplanet. Currently, the highest altitude of long-term human colonization is on the Tibetan Plateau at around 4,500 m, where the density of the atmosphere is around 60% of that at sea level. The partial pressure of oxygen experienced here is equivalent to being at sea level on a planet with only ~12.5% O_2 in its atmosphere. A selection of metabolic traits acquired over more than 6,000 years of permanent human habitation of the plateau (Horscroft et al. 2017) have made complex, intelligent life here possible. This level of atmospheric oxygen abundance is roughly what is thought to be required for oxygen to penetrate deep into the ocean interior (Canfield 1998). Thus, given that our main constraint on pre-Silurian atmospheric oxygen levels is the persistence of marine anoxia (Sperling et al. 2015), it is possible that an atmospheric oxygen concentration sufficient for highly adapted modern humans may have been available throughout the entire Phanerozoic and perhaps even into the Proterozoic.

Aerobic respiration: the chemical process by which oxygen reacts with carbohydrates to generate energy

Exoplanet: a planet that is outside of our Solar System; it may or may not orbit another star

Fully resolving the questions around how O_2 levels have influenced animal evolution and at what stage animals, including humans, might have been able to colonize Earth requires more detailed tools for tracking atmospheric oxygen levels through Phanerozoic time. In this review we give an overview of the global oxygen cycle, discuss the currently available methods to track and reconstruct Phanerozoic O_2 levels, and attempt to produce a general consensus view supported by the most reliable methods.

2. WHAT CONTROLS O_2 LEVELS IN THE ATMOSPHERE AND OCEAN?

It is possible to produce molecular oxygen when water or carbon dioxide molecules are split by the Sun's rays in the upper atmosphere (photolysis), which is why Mars's very thin atmosphere has an O_2 mixing ratio of about 0.17% (Franz et al. 2017). The buildup of an ozone layer during the Paleoproterozoic Era would have curtailed this process, and the only other way to produce large amounts of molecular oxygen is through biological means: oxygenic photosynthesis. Photosynthesis has been active on Earth for at least 2.7 billion years, and perhaps much longer (Buick 2008), and has effectively produced all of the oxygen that is in the atmosphere and oceans today. However, the accumulation of O_2 in the atmosphere is not simply a matter of determining rates of photosynthesis. As shown in **Figure 1**, almost all of the oxygen generated through photosynthesis (more than 99%) is consumed rapidly during aerobic respiration (e.g., Hedges & Keil 1995). In the ocean, organic material is constantly produced through photosynthesis and is respired as it sinks through the water column. This results in oxygen minimum zones (OMZs or dead zones) where the oxygen demand for respiration reduces the oxygen availability in the water column. On land, plants themselves respire the O_2 they produce, as do the soil communities. However, neither of these environments allows for the complete respiration of all the organic matter initially produced, resulting in the burial and preservation of organic carbon.

The tiny fraction of organic carbon that is buried is responsible for the rise of oxygen to modern levels (Garrels & Perry 1974). During photosynthesis, 1 mole of O_2 is produced when converting 1 mole of CO_2 to organic material; thus, every mole of organic carbon that is preserved represents 1 mole of O_2 that remains free in the surface environment. This picture is complicated by

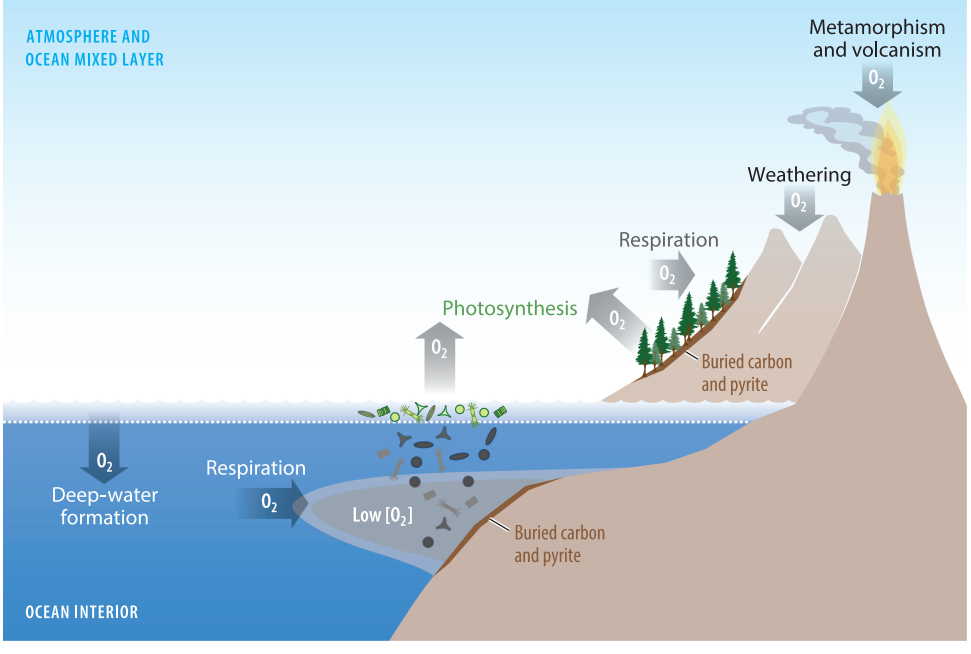

Figure 1

The global oxygen cycle. The short-term cycle of photosynthesis and respiration involves large fluxes but ultimately produces a small net source of O_2 proportional to the amount of buried carbon and pyrite. The long-term cycle balances this net source with the weathering and metamorphism of these carbon- and pyrite-containing sediments.

other processes that occur in the sediments or soils once oxygen has been consumed. Microbes do not need to use aerobic respiration to derive energy from organic matter and may instead process the organic carbon through other avenues, e.g., sulfate reduction, where the terminal electron acceptor (i.e., the molecule where the oxygen is coming from) is SO_4 rather than O_2. In this way the organic carbon is converted to CO_2 and not buried, but no O_2 has been consumed. Fortunately, for the purpose of tracking O_2 fluxes, sulfate reduction produces hydrogen sulfide, which readily reacts with iron to form pyrite, and thus every mole of pyrite sulfur buried in sediments represents ~2 moles of photosynthetic O_2 that remains in the surface environment. There are, of course, other consumption fluxes of O_2 aside from respiration, and in the long-term carbon cycle the net O_2 source linked to carbon and pyrite burial is matched by the sinks through oxidation of fossil organic carbon or pyrite sulfur in ancient sediments, either directly during exposure and weathering or through metamorphism (Garrels & Perry 1974, Berner 2004). Several methods for reconstructing atmospheric oxygen abundance rely on reconstructing these sources and sinks of O_2. Others use information that pertains directly to the atmospheric O_2 concentration, to the marine O_2 concentration, or to other aspects of the global carbon cycle that are linked to O_2.

3. LONG-TERM O_2 CONSTRAINTS

Before we assess the Phanerozoic record of atmospheric oxygen, we summarize the wider context of the rise in atmospheric O_2 over Earth history, as this sets key boundaries for any Phanerozoic reconstruction. **Figure 2** shows the key long-term constraints on atmospheric O_2 levels. Before the Great Oxidation Event during 2400–2200 Ma, atmospheric oxygen concentrations were less than 1 ppm, which is known with some certainty because of abundant evidence for the mass-independent fractionation of sulfur isotopes (MIF-S) in all samples before 2400 Ma (Farquhar et al. 2000). Usually processes that separate isotopes of an element do so in ways related to the mass of each isotope, but some photochemical atmospheric reactions (i.e., using UV radiation from the Sun) can produce mass-independent effects and are only possible in an atmosphere almost completely devoid of oxygen (Gregory et al. 2021). This explanation is further supported

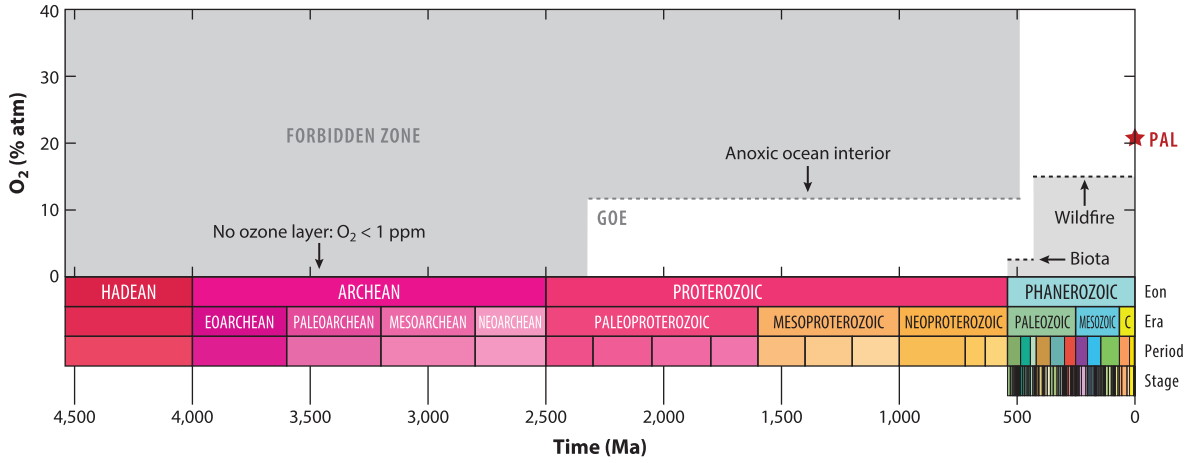

Figure 2

Long-term constraints on atmospheric O_2 over Earth history. Upper limits are set by the mass-independent fractionation of sulfur before ~2400 Ma and by broadly anoxic bottom waters until the Ordovician. Lower limits are set by the requirements of the animal biota in the early Paleozoic and then by the existence of wildfires from ~430 Ma to present. See the text for details of these limits. Abbreviations: C, Cenozoic; GOE, Great Oxidation Event; PAL, present atmospheric level.

by a plethora of redox-sensitive tracers that determined the weathering zone and shallow marine environment to be largely devoid of oxygen at this time (Catling & Zahnle 2020) and also by marine redox tracers that show that oxygen penetration into the marine environment increases at the time when the MIF-S record disappears (Poulton et al. 2021).

From the Great Oxidation Event through to the Cambrian, an upper limit on oxygen levels of about 12% of the atmosphere (close to half of today's level) is determined based on the persistence of widespread anoxia in the ocean interior (**Figure 2**). Anoxia is determined principally here through the speciation of iron minerals in shales throughout the Proterozoic and Cambrian (Sperling et al. 2015), where deeper water samples show a dominance of highly reactive phases that are only found in such quantities in sediments overlain by anoxic water (Poulton & Canfield 2005). The association of deep ocean anoxia with atmospheric O_2 levels less than ~12% atm is based on simple box-modeling of the supply and demand of oxygen in the water column (e.g., **Figure 1**). The present-day O_2 supply exceeds the demand for respiration of sinking organic matter and thus the ocean interior is oxic, but this would not be the case if the mixed layer O_2 concentration were reduced by about half (Canfield 1998, Watson et al. 2017). Recent 3D modeling work has shown that due to changing ocean circulation under different continental configurations, substantial parts of the deep ocean could have been anoxic in the early Paleozoic even under present-day atmospheric O_2 levels (Pohl et al. 2022). Nevertheless, the continental shelves, where the geochemical data supporting anoxia are found, tend to remain relatively well oxygenated in these simulations. Further work with 3D models is required to better constrain atmospheric oxygen levels using marine geochemical records.

The lower limit for oxygen associated with the demands of Ediacaran and Cambrian biotas is also a useful benchmark for minimum O_2 levels and sits at around 0.2% in the Ediacaran and around 2% in the Cambrian (Sperling et al. 2015). These were determined through an assessment of the O_2 demands of present-day sponges [as analogs to the Ediacaran biota (Mills et al. 2014)] and OMZ seafloor animals (Levin 2003). A much more certain lower limit exists from the mid-Silurian onward and is defined by the presence of inertinite in sediments between 430 and 0 Ma. Inertinite is a by-product of wildfires, which require high levels of oxygen to proliferate. Experiments have determined that fires cannot sustain themselves below 15% O_2, setting a clear lower limit for much of the Phanerozoic (Belcher & McElwain 2008, Belcher et al. 2013, Glasspool & Gastaldo 2022). There are periods after the charcoal record begins (e.g., during the Devonian, the Early Triassic, and the very Early Cretaceous) when inertinite is sparsely recorded or absent, and it is uncertain if this is related to low pO_2 or unfavorable conditions for preservation (Scott & Glasspool 2006, Diessel 2010, Glasspool & Scott 2010).

Inertinite: fossilized charcoal, usually derived from the pyrolysis of wood, but can sometimes contain the charred remains of seeds, flowers, and fungal cells

4. METHODS OF PHANEROZOIC O_2 ESTIMATION

We group the O_2 reconstruction methods into those that infer oxygen concentration in the atmosphere directly, those that rely on changes in marine redox to infer atmospheric O_2, and those that are based on broader aspects of Earth's global elemental cycles. These are shown in **Figure 3*a–c***, respectively. In this figure, O_2 reconstructions that are generally consistent with the long-term constraints from Section 3 are colored in blue or green, whereas reconstructions that clearly violate the constraints are colored in orange or yellow. Isotope mass balance (IMB) techniques are discussed separately in Section 5.

4.1. Direct Atmospheric Methods for Atmospheric O_2 Reconstruction

The following methods are based on attempts to sample ancient air directly or to record aspects of the terrestrial environment that are strongly linked to atmospheric oxygen, such as the prevalence

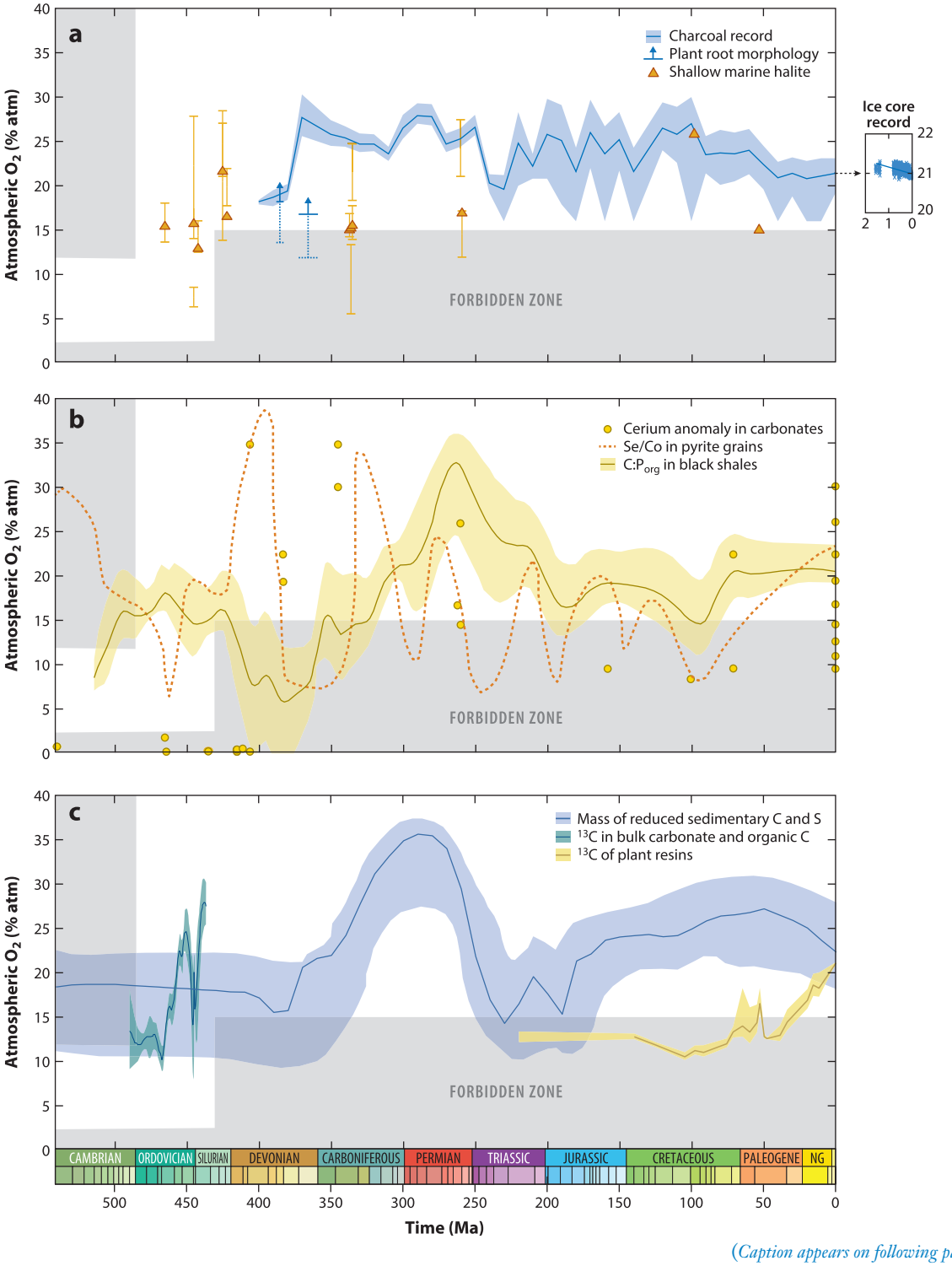

(*Caption appears on following page*)

Figure 3 (*Figure appears on preceding page*)

Phanerozoic O_2 estimates from geological and geochemical proxies. (*a*) Direct proxies for atmospheric composition (Section 4.1). (*b*) Proxies related to marine oxygenation related to atmospheric O_2 (Section 4.2). (*c*) Sediment abundance and isotopic fractionation methods (Section 4.3). Blue/green colors denote estimates that will form part of our combined estimate; yellow/orange colors denote estimates that will not. See the listed text sections for further details and discussion of these methods. The gray areas show the forbidden zone from **Figure 2**. Abbreviation: NG, Neogene.

of wildfires and the oxygen concentration in soils. These proxies have great potential for accurate reconstruction but generally suffer from poor spatial coverage and time resolution.

4.1.1. Ice core records. The clearest way to estimate past levels of oxygen in the atmosphere is from ice core records, which contain samples of ancient air trapped in bubbles within the ice. This method has been famously used to determine ancient CO_2 levels over the Quaternary period (e.g., Petit & Raynaud 2020), and current estimates of oxygen concentration from ice core samples indicate that pO_2 has declined from ~21.14% to ~20.95% of the atmosphere over the past 1.5 Myrs (Stolper et al. 2016, Extier et al. 2018, Yan et al. 2019). This is shown as an inset in **Figure 3*a***, as the relatively short time span is not easily visible when looking at the whole Phanerozoic. Ice core records are currently not available beyond about 2.7 Ma (Yan et al. 2019); thus, despite their incredible fidelity, their usefulness in determining Phanerozoic-scale O_2 variations is limited.

4.1.2. Halite gas inclusions. Halite is a mineral that is formed when seawater evaporates. This process can result in fluid inclusions in the halite minerals, derived from the original body of water. Within those fluids it is possible to find bubbles of trapped air. A rigorous screening process has been developed to ensure that these fluid inclusions and gas bubbles have the best chance of reflecting the atmospheric composition of the time (Blamey & Brand 2019), and the Phanerozoic samples collected so far that meet these criteria (from Blamey et al. 2016, Brand et al. 2021) are shown in **Figure 3*a*** and coarsely span the Ordovician to Paleogene. Uncertainty was calculated by assessing concentrations of oxygen versus organic matter–derived gases in the samples in order to estimate the original O_2 concentration before any reactions took place. This can generate a large uncertainty window, and in some cases samples of the same age have nonoverlapping uncertainties (Brand et al. 2021) (**Figure 3*a***), which may indicate problems with preserving original signals or with the method used to back calculate the original composition.

A potential problem with the method appears most clearly when looking at samples from the Archean, which indicate an atmospheric O_2 level of 3% atm—one-seventh of the present-day level (Steadman et al. 2020). This is vastly higher than the upper limit of one-millionth of the present-day level (**Figure 2**) set by the Archean MIF-S record (Farquhar et al. 2000), and the similar upper limits set by the absence of iron oxides, the presence of detrital reduced minerals that would be oxidized at even low atmospheric O_2 (Rasmussen & Buick 1999, Holland 2006, Kump et al. 2013), and a lack of isotope fractionation in elemental cycles (Cr, Mo, U) that readily produce these signals in the presence of oxygen (see Catling & Zahnle 2020). Thus, while the potential to sample ancient air makes this method appear very promising, this issue of major disagreement with the overwhelming majority of Archean O_2 estimates remains to be resolved.

4.1.3. The charcoal record. Fossil charcoal is an indicator that wildfires occurred in the geological past (Scott 1989, Scott & Jones 1991). Dead vegetation undergoes peatification and then coalification, with the resultant coal composed of different groups of macerals, dependent on the method of breakdown (e.g., physical, chemical, bacterial). One maceral group—inertinite, which fusinite (mostly fossil charcoal) belongs to—is formed primarily due to pyrolysis of vegetation by wildfires (Scott 1989, Scott & Jones 1991, Scott & Glasspool 2007). As well as oxygen, wildfires

Halite: commonly known as rock salt, with the formula NaCl

require heat, fuel, and an ignition source, such as lightning strikes, which themselves can be identified in the fossil record (e.g., Cope & Chaloner 1980, Scott & Jones 1991, Pyne et al. 1996). The presence of inertinite in the geologic record indicates that there was sufficient oxygen in the atmosphere to sustain wildfires for much of the past ~430 Myrs (Glasspool & Gastaldo 2022), but there have also been attempts to use the fossil charcoal record to generate quantitative estimates of Phanerozoic pO_2. A database of the percentage by volume of inertinite in coals (Inert%, e.g., normalized to the volume of coal) was collated, binned into 10 Myr intervals, and used to calculate pO_2 by generating calibration curves and deriving a power law relationship (Glasspool & Scott 2010). At 21% O_2 the mean Inert% is 4.3% (based on Pleistocene to Recent samples), and it was assumed that with an Inert% of 0.2% (equivalent to a single charcoal particle in a coal sample), this would equal the experimental minimum O_2 of 15% atm (Belcher & McElwain 2008). A maximum abundance of inertinite occurs during the early Permian (280 Ma), where Inert% is 44.4%, and this was assumed to correspond to a pO_2 level of 30% atm, beyond which it was predicted that fires would be so widespread as to limit any further oxygen rise through limitation of photosynthetic productivity. An update to the method, using S-shaped calibration curves instead, was applied to the Paleozoic by Glasspool et al. (2015). Here we use the updated method to recalculate the Mesozoic and Cenozoic data from Glasspool & Scott (2010) and plot the results in **Figure 3*a***. Overall, the charcoal curve describes a rise in O_2 levels during the Devonian, high levels in the Carboniferous–Permian, and a long decline between the Cretaceous and the present day.

4.1.4. Fossil plant root morphology. Plants require oxygen to perform aerobic respiration. Specifically, the roots must respire in order to take up nutrients, and for tissue maintenance and growth, thus setting a minimum oxygen concentration in the soil at the root depths. A new method (Sønderholm & Bjerrum 2021) uses a soil-root model to calculate the drawdown of O_2 from the atmosphere to the soil, based on the known depth of plant roots in the past and the soil medium. This is then used to infer atmospheric O_2 levels. Currently this method has only been applied to *Archaeopteris*, an extinct link between the ferns and the gymnosperms (nonflowering, seed-producing plants) that lived during the Devonian and Carboniferous (Sønderholm & Bjerrum 2021). The calculated O_2 required for optimal growth is around 17% atm, shown in **Figure 3*a***. It is possible that *Archaeopteris* could have survived at ~12% O_2 as an absolute lower limit, but the evidence for wildfire suggests that O_2 levels were 15% or higher.

4.2. Atmospheric O_2 Inferred from Marine Redox Proxies

Marine sediments are plentiful throughout the Phanerozoic, and a large number of proxy tools have been developed to infer the redox state of the overlying water column, or the global ocean, from either enrichments, distribution of an element between different species, or isotope fractionations. As detailed in Section 3, iron speciation has documented widespread anoxic seafloor conditions before the Ordovician (Sperling et al. 2015) that are used to infer an upper limit for atmospheric O_2 levels during this time. Some studies have sought to use marine redox proxies to make quantitative estimates of the changes in atmospheric O_2 levels throughout the Phanerozoic. All of these methods are in conflict with the lower limit set by the charcoal record, and we attribute this mismatch to the difficulty in extrapolating precise atmospheric O_2 levels from marine oxygenation. The ocean is a tiny reservoir of oxygen compared to the atmosphere, holding less than 1% of the surface O_2 budget. Also, marine redox is highly spatially variable and is controlled at the local scale by the availability of organic matter and O_2 consumption by respiration (see **Figure 1**). Finally, the preserved sediment record, particularly pre-Jurassic, is strongly biased toward shallow marine epicontinental seas, which have an unclear relationship to conditions in the wider ocean. Given these uncertainties and others, most marine redox proxies have not been converted into a

quantitative estimate of atmospheric O_2 levels, but the few that have are explored below and are plotted in **Figure 3*b***.

4.2.1. Cerium anomalies in carbonate sediments. Ce is a rare earth element (REE), a group of metals with similar properties but with sufficient differences to make the ratio of one REE to another a useful metric. Specifically, Ce, unlike the other REEs, can be removed from solution by oxidation. This means that calculating a Ce depletion relative to the other REEs in carbonate sediments (a negative Ce anomaly) can indicate the presence of oxygen in the water column. Ce anomalies have been used as a qualitative metric for late Neoproterozoic and Phanerozoic oxygenation (Wallace et al. 2017), while a quantitative method calculates atmospheric O_2 concentrations from the Ce anomaly by assuming that shallow-water carbonates precipitate in environments in equilibrium with the atmosphere; thus, the concentration of Ce can be related to atmospheric O_2 (Liu et al. 2021). The concentration of Ce is then related to the Ce anomaly by assuming other REE concentrations did not change over time. Both qualitative and quantitative analyses show a broad shift toward greater Ce anomalies during the Devonian, but the quantitative method predicts O_2 levels as low as ~0.2%, in contradiction to the inertinite record, at the start of the Devonian. It should be noted that Liu et al. (2021) were mostly concerned with calculating these concentrations over the Precambrian, for which their order-of-magnitude approach is more appropriate.

4.2.2. Carbon to phosphorus ratios in black shales. Organic matter from marine primary producers tends to comprise C and P in the ratio 106:1 (Redfield 1958). Some of this organic matter eventually sinks to the sediments (e.g., **Figure 1**), where much of it is oxidized by microbes, transforming the carbon to CO_2 and releasing the P. Because microbes often focus on P-rich compounds, P is preferentially released during this process, leaving the remaining organics P depleted (Algeo & Ingall 2007). Further redox-dependent processes can then occur in the sediment, which may trap this newly liberated P, affecting the overall C_{org}:$P_{reactive}$ measured in the sediments (i.e., the ratio of organic carbon to soluble P). In general, high C_{org}:$P_{reactive}$ indicates that P has been recycled back to the water column, and low C_{org}:$P_{reactive}$ suggests that P has been retained in the sediments. P retention in sediments is a strong function of oxygen availability, as much of the P trapping occurs through the formation of iron oxyhydroxides (Van Cappellen & Ingall 1994). Thus, when considering organic-rich (black) shales at the global scale, the degree of P trapping (tendency for a low C_{org}:$P_{reactive}$) may be related to the oxygenation of the oceans in general, which can be related to oxygen supply from surface waters equilibrated with the atmosphere. This was the approach of Algeo & Ingall (2007), who used records of C_{org}:P_{total} in sediments as a proxy for C_{org}:$P_{reactive}$ and scaled the resulting qualitative O_2 curve to ensure it did not violate the constraints imposed by the existence of fossil charcoal (Wildman et al. 2004). More recent works on wildfires and the charcoal record (Belcher & McElwain 2008, Glasspool et al. 2015, Glasspool & Gastaldo 2022) have subsequently meant that the predicted O_2 curve no longer satisfies these constraints.

4.2.3. Selenium to cobalt ratios in pyrite grains. Se is sourced through the oxidative weathering of sulfide minerals. Therefore, the marine Se concentration is expected to increase when atmospheric O_2 levels are greater. Conversely, Co concentrations are expected to decrease when the ocean is oxygenated due to adsorption onto iron oxyhydroxides. Large et al. (2019) proposed that marine Se and Co concentrations are reflected in the concentration of these elements in sedimentary pyrite, where Se can substitute for S and Co can be incorporated into the crystalline structure. They derived a proxy for atmospheric oxygen by dividing Se concentration by Co concentration and scaling this at points in the Neoproterozoic and Phanerozoic to atmospheric O_2 reconstructions from other methods. A recent revision of this parameterization instead uses a

power law to relate Se and Co concentrations to atmospheric O_2 (Cannell et al. 2022). **Figure 3*b*** shows the best guess curve of Large et al. (2019) for the Phanerozoic. This reconstruction is not consistent with the charcoal record as it records several dips to very low atmospheric O_2 at times where wildfire was abundant (Glasspool et al. 2015). The revised formulation is not plotted as it has only been produced for the Paleozoic, but it too falls below the wildfire minimum (Cannell et al. 2022). Sulfide weathering has a weakening dependence on oxygen concentration when oxygen levels are high and may be more dependent on erosion rates (Daines et al. 2017) and the action of the biosphere (Kanzaki & Kump 2017). This could help explain why these O_2 reconstructions record rising O_2 levels over the Cenozoic, when global erosion rates are increasing.

4.3. Atmospheric O_2 Inferred from Sedimentary Abundances and Isotope Fractionations

These methods (**Figure 3*c***) are based on Earth's long-term carbon cycle and seek to reconstruct variations in atmospheric O_2 either directly from the burial rates of organic carbon and pyrite (the long-term O_2 sources; see Section 2) or from the carbon isotopes of organic material, which can be related to photosynthesis—which is sensitive to the atmospheric O_2:CO_2 ratio.

4.3.1. Sedimentary carbon and sulfur masses. Given that the total flux of O_2 production over geological time is related to the combined burial of organic carbon and pyrite, a simple but effective way to estimate the accumulation of O_2 in the atmosphere is to record the mass of these species in sediments around the world over the Phanerozoic. Berner & Canfield (1989) set out to do this by using existing global sediment records and their average C and S compositions to determine organic carbon and pyrite burial rates through time (Ronov 1976, Budyko et al. 1987). Pyrite burial rates were constrained by adding an oxygen dependency, as the record of marine sediments did not include redox information. More pyrite burial is expected in anoxic and sulfide-rich conditions, which are more prevalent at low O_2. This increases O_2 production, and thus net pyrite burial starts to decrease, resulting in a strong negative feedback on O_2 levels from the S cycle. Consumption fluxes, through the weathering of organic carbon and pyrite, were also computed and were based on sediment accumulation rates. The resulting atmospheric O_2 prediction has a large uncertainty, as one might expect given the generalized nature of the method. Nevertheless, the curve is consistent with the long-term constraints, although they suggest the very minimum of the uncertainty window should be taken during the Cambrian. The strong negative feedback from the S cycle may be why the best guess model does not predict less than 15% O_2 at any point in the Phanerozoic.

4.3.2. Carbon isotopes in plant resins. Photosynthesis converts carbon dioxide and water into oxygen and organic carbon. However, the reaction can also proceed in the opposite direction and consume oxygen—photorespiration—and the ambient O_2 concentration is a major factor in determining how efficient photosynthesis is. Tappert et al. (2013) used fossil plant resins (e.g., amber) as a $\delta^{13}C$ archive of plant materials over time to estimate changes in atmospheric O_2 based on this photosynthetic efficiency. They opted to use a direct proportionality between isotopic fractionation and O_2 levels, rather than a laboratory-measured curve for isotopic fractionation at different O_2 levels (Berner et al. 2000), because the degree of fractionation was much smaller than Berner et al. (2000) obtained. Their reconstructed O_2 curve falls well below the wildfire limit for much of the Mesozoic. This may be due to uncertainties in what is controlling plant resin $\delta^{13}C$ values, given that precipitation can impart differences of up to 6‰ (Diefendorf et al. 2012), similar to the measured range in Tappert et al. (2013), and might explain smaller fractionation in the Mesozoic where precipitation was restricted on the supercontinent Pangea (e.g., Otto-Bliesner 1995).

4.3.3. Measuring photosynthetic response to O_2 levels. Changes in photosynthetic efficiency, as discussed in Section 4.3.2, also impact the isotopic composition of the organic carbon created. Laboratory experiments have determined relationships between O_2 levels and the isotopic fractionation (i.e., change in isotopic composition) imparted by photosynthesis (Berner et al. 2000, Beerling et al. 2002). Therefore, the isotopic composition of carbon in the geological record can be used to estimate O_2 levels. Edwards et al. (2017) used paired isotope values from organic and inorganic carbon in Ordovician sediments to estimate this photosynthetic effect directly and therefore make a prediction for atmospheric O_2 levels. Their results indicate a rise in O_2 levels, which is consistent with the long-term constraints.

4.4. O_2 Reconstructions Using Isotope Mass Balance

IMB is a technique that aims to reconstruct the global O_2 source from sedimentary isotope ratios, rather than from rock masses. The advantage over the rock mass method is that isotopic information is available in high fidelity throughout Phanerozoic time and is not clearly influenced by the poor preservation of more ancient sediments or changing average compositions of sediment types. The method hinges on the isotopic discrimination imparted by photosynthesis, which leaves the $\delta^{13}C$ value of organic carbon around 27‰ lighter than the CO_2—or marine bicarbonate—from which it is derived, although many factors, including O_2 levels as mentioned previously, can alter this (Berner et al. 2000, Beerling et al. 2002). With knowledge of the isotopic composition of the global inorganic carbon reservoir (recorded in carbonate rocks) and of the isotopic composition of global carbon inputs (i.e., volcanic CO_2), it is possible to calculate the fraction of total carbon burial that was organic. Knowing that total carbon burial must equal the total carbon input over long timescales, the organic carbon burial rate and net production of O_2 can be calculated:

$$BC_{org} = BC_{total} \times \left(\delta^{13}C_{carb} - \delta^{13}C_{input}\right)/\Delta C, \quad 1.$$

where BC_{org} is the global organic carbon burial rate, BC_{total} is the total (organic plus inorganic) carbon burial rate, $\delta^{13}C_{carb}$ is the carbon isotopic composition of carbonate rocks, $\delta^{13}C_{input}$ is the average carbon isotopic composition of volcanic CO_2 and all carbon weathering, and ΔC is the photosynthetic fractionation factor (around −27‰).

This IMB approach was first derived by Garrels & Lerman (1984) and then employed in several papers by Berner (1987, 2001), ultimately forming the basis of the GEOCARBSULF model for atmospheric O_2 over Phanerozoic time (Berner 2006). In these papers a sulfur cycle IMB was also employed alongside the carbon IMB shown above, in order to calculate pyrite burial rates. The sulfur cycle has a similar isotope discriminating process—sulfate reduction—which makes buried pyrite around 35‰ lighter than the seawater sulfate from which it was derived:

$$BS_{pyr} = BS_{total} \times \left(\delta^{34}S_{sw} - \delta^{34}S_{input}\right)/\Delta S, \quad 2.$$

where BS_{pyr} is the global pyrite burial rate, BS_{total} is the total (pyrite plus gypsum) sulfur burial rate, $\delta^{34}S_{sw}$ is the sulfur isotopic composition of seawater (reflected in the composition of sulfate minerals), $\delta^{34}S_{input}$ is the average sulfur isotopic composition of both volcanic and weathering derived sulfur, and ΔS is the sulfate reduction fractionation factor (around −35‰).

Both the carbon and sulfur cycles employed in the GEOCARBSULF model are shown in **Figure 4*a***. Because the total rates of carbon and sulfur input into the atmosphere and oceans are required to calculate the O_2 source, and because processes that consume O_2 must also be considered, the model is run forward in time. The model is subject to an assumed global CO_2 degassing rate and calculates surface processes such as continental weathering in response to global temperature change. It estimates the isotopic composition of each crustal reservoir, the input and output fluxes, and the amount of O_2 and CO_2 in the atmosphere and ocean at each timestep in

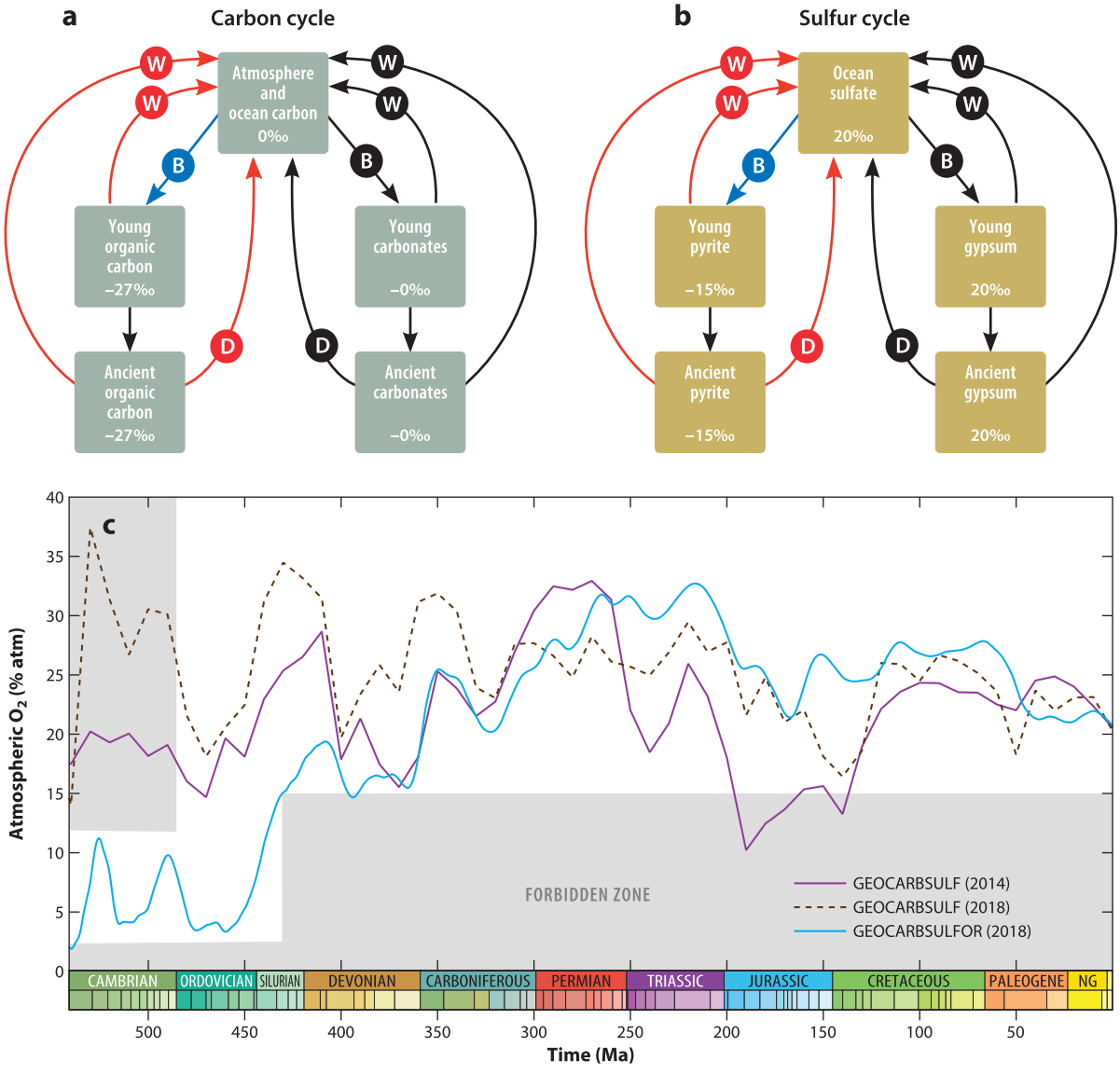

Figure 4

IMB techniques. (*a*) Schematic of the long-term carbon cycle as used in IMB modeling. (*b*) Schematic of the long-term sulfur cycle as used in IMB modeling. (*c*) Atmospheric O_2 predictions from IMB models. The purple line shows the GEOCARBSULF model of Royer et al. (2014). The brown dashed line shows an update using a more recent carbon isotope record to drive the model (Schachat et al. 2018). The light blue line shows the same newer carbon isotope record plus an update to the model structure as by Krause et al. (2018). See the text for further details. The gray areas show the forbidden zone from **Figure 2**. Abbreviations: B, burial; D, degassing; IMB, isotope mass balance; W, weathering.

accordance with the modeled processes. For a more detailed review of GEOCARBSULF, see Berner (2006), Royer et al. (2014), and Mills et al. (2019).

Figure 4*c* shows the Phanerozoic O_2 predictions from recent versions of the GEOCARBSULF model. Royer et al. (2014) (purple line, **Figure 4**) updated Berner's original methodology with new

estimates for continental weathering, and their results are similar to the O_2 trends that the model has produced since the initial 2006 version. The model has always predicted near present-day oxygen levels in the early Paleozoic, a Permo-Carboniferous maximum, and a dip to low values either close to or below the fire minimum at around 200–150 Ma (Belcher & McElwain 2008, Berner 2009). These O_2 predictions show some clear similarities to the carbonate $\delta^{13}C$ and sulfate $\delta^{34}S$ records that were used to drive the model. In general theory, higher $\delta^{13}C$ values in carbonates reflect heavier seawater values, which can be a product of higher rates of photosynthesis and carbon burial removing the lighter isotope. Similarly, higher sulfate $\delta^{34}S$ values are generally interpreted as higher rates of pyrite burial, which also denotes a net source of O_2. The IMB equations shown above are consistent with these statements, but the calculated O_2 flux may also be altered if, for example, the isotopic composition of carbon or sulfur inputs were to change.

While Royer et al. (2014) had updated the $\delta^{34}S$ record to use data compiled by Wu et al. (2010), it was not until 2018, almost a decade after Berner's final contribution, that the $\delta^{13}C$ input data were revised (Schachat et al. 2018) (brown dashed line, **Figure 4**). This update changed the model predictions substantially, raising O_2 levels clearly above the fire minimum in the Mesozoic and removing the prominent Permo-Carboniferous maximum. This modification also substantially increased the predicted oxygen concentration in the early Paleozoic, to above 35% during the Cambrian, which is difficult to reconcile with a long-term persistence of marine anoxia (Sperling et al. 2015). Contradictory behavior like this in the early Paleozoic spurred an investigation into the processes responsible, which led to the model revision by Krause et al. (2018) (blue line, **Figure 4**).

As discussed above, $\delta^{13}C$ fractionation during photosynthesis is dependent on atmospheric O_2 concentrations, with greater fractionation occurring at higher O_2 levels. Practically, this means that as O_2 increases in the model, ΔC increases in Equation 1, and the burial rate of organic carbon calculated to satisfy the isotope record decreases. Berner (2001) added a similar but much stronger effect to pyrite burial in the model, with $\delta^{34}S$ fractionation also dependent on atmospheric O_2. This was based on observations for increased fractionation when sulfide reoxidation was a major component of the sulfur cycle (Canfield & Teske 1996). However, both the relationship of reoxidation to O_2 levels and the necessity for this process to drive large isotopic fractionations are uncertain (Jørgensen & Nelson 2004, Sim et al. 2011, Krause et al. 2018). The strength of the feedback function applied in GEOCARBSULF was such that an atmospheric O_2 mixing ratio of 2.5% (i.e., the minimum required for the Cambrian biota) would result in a $\delta^{34}S$ fractionation factor of around 4‰, far below anything recorded during the Phanerozoic, and implying a massive rate of pyrite burial and net O_2 production in order to fit the isotopic data.

Krause et al. (2018) removed the IMB for pyrite burial and replaced it with a forwards method, calculating pyrite burial rates from the availability of organic matter, sulfate, and oxygen. Instead of using the geological sulfur isotope record as an input, the model could predict the $\delta^{34}S$ of sulfates, and this was compared with the geological record (Krause et al. 2018). This version of the model was renamed GEOCARBSULFOR—reflecting the forwards sulfur cycle—and while the Mesozoic and Cenozoic results were similar to those of Schachat et al. (2018), the early Paleozoic O_2 levels were considerably lower, in line with the long-term O_2 constraints. Because of the highly detailed carbonate $\delta^{13}C$ record, IMB is able to produce the highest resolution O_2 reconstructions of any method available. Nevertheless, the method relies on a series of important assumptions and data sets and therefore still has high uncertainty.

4.5. Forwards Models of Atmospheric O_2

A forwards (or predictive) model is one in which only the most basic tectonic and evolutionary boundary conditions are defined from the geological record, and the model attempts to predict from there the evolution of the Earth system using process-based descriptions of global

biogeochemistry and climate (e.g., COPSE: Bergman et al. 2004, Lenton et al. 2018; MAGic: Arvidson et al. 2013; SCION: Mills et al. 2021). Here, oxygen production is controlled directly by biological productivity and carbon burial, which is dependent on the liberation of nutrients through continental weathering. These models produce predictions of Phanerozoic atmospheric O_2 levels. However, the purpose of these models is to understand what drives changes in the Earth system, and their predictions were never intended to be used as best guess scenarios for atmospheric O_2. Thus, we do not include the results of these models in this attempt to establish consensus over atmospheric O_2 evolution.

5. TOWARD A CONSENSUS CURVE FOR PHANEROZOIC ATMOSPHERIC O_2

We now try to combine what we know about atmospheric O_2 variation over Phanerozoic time into a single curve and uncertainty window. We believe such a curve is needed due to a rapid expansion in available methods to reconstruct O_2 (see Section 4), combined with a tendency in the literature to plot forwards model outputs (Arvidson et al. 2013, Lenton et al. 2018), obsolete model versions (Bergman et al. 2004, Berner 2006), or even studies that test the limits of models (Zhang et al. 2018) in place of genuine O_2 reconstructions. This section introduces our first attempt at this curve. Because of the very high time resolution possible, and the lack of any clear disagreement with the long-term constraints, we use the IMB O_2 predictions as the central line in this curve but expand the uncertainty window to cover all of the current methods that themselves do not violate the long-term constraints. In this way, a best guess for both short- and long-term O_2 variations can be made.

5.1. Update to the Isotope Mass Balance Approach

Because IMB depends on the $\delta^{13}C$ record, as well as (for example) reconstructions for tectonic CO_2 degassing rates, it is necessary to update these input parameters when new data become available. We do this within the GEOCARBSULFOR model, rather than GEOCARBSULF, due to the aforementioned uncertainty and violation of the long-term constraints on O_2 from the sulfur cycle in the original GEOCARBSULF (Krause et al. 2018). We have updated GEOCARBSULFOR further here by running Monte Carlo simulations to produce an envelope of uncertainty (as in Royer et al. 2014). We vary five key variables that have a high degree of control over predicted O_2 levels: uncertainty in the long-term records of $\delta^{13}C_{carb}$, tectonic degassing, continental erosion, the assumed climate sensitivity to changes in CO_2 levels, and the scaling coefficient that links changes in photosynthetic $\delta^{13}C$ fractionation to atmospheric O_2. For these five variables we sample equally between maximum and minimum bounds, running the model 5,000 times by utilizing MATLAB's parallel computing toolbox. Code to perform single runs of the model, and the Monte Carlo procedure, is freely available at **https://github.com/Alexjkrause**. This web page also includes the model equations, which can also be found in Krause et al. (2018). The present model updates are detailed below.

5.1.1. The $\delta^{13}C_{carb}$ record. The $\delta^{13}C_{carb}$ record is used to infer the $\delta^{13}C$ composition of seawater across the Phanerozoic and is employed to calculate the organic carbon burial flux through IMB. In the previous version of GEOCARBSULFOR (hereafter GEOCARBSULFOR-2018) (Krause et al. 2018), this was based on the compilation by Saltzman & Thomas (2012). The data from 540 Ma to present were placed into 5 Myr bins, and a 10 Myr moving average was applied to generate an average record. The $\delta^{13}C$ value at 540 Ma was used for the model spin-up phase (570–540 Ma). For our update, we now use the compilation of Cramer & Jarvis (2020). We place

the data from 538.8–0 Ma into 2 Myr bins and calculate an average and $\pm 1\sigma$ as the uncertainty range for the Monte Carlo ensemble (**Figure 5*a***).

The higher fidelity of the new record and our smaller bins allow the model input curve to faithfully represent the variations in $\delta^{13}C_{carb}$ on the approximately million-year timescale. This record is assumed by the model to represent the average carbon isotope composition of the ocean, but this is not completely straightforward, as the Paleozoic record is almost entirely from epicontinental (inland) seas, due to the subduction of most records deposited in deeper waters. Such environments can develop $\delta^{13}C$ values around 1‰ or perhaps a maximum of 2‰ higher than the ocean mean. The record we use here was constructed based on the principle that it should reflect mean ocean values, ensuring there was no clear step change in the isotope record when it switched to records from deeper settings (Cramer & Jarvis 2020).

5.1.2. Tectonic degassing. Normalized degassing rates were used in GEOCARBSULFOR-2018 to help generate estimates of carbon or sulfur emissions to the ocean-atmosphere system from the combination of tectonism and metamorphism. These were based on seafloor spreading, as a general approximation to degassing at both mid-ocean ridges and subduction zones. The rates for 0 to 150 Ma were calculated by using data from Engebretson et al. (1992), and earlier rates were based on the sea-level record, which was inverted to produce ridge volumes and thus degassing rates (Gaffin 1987). Since then, improved estimates of degassing have been made through full-plate modeling (Domeier & Torsvik 2017) and compilations of the extent of volcanic arcs (Mills et al. 2017) and rifts (Brune et al. 2017). In the revised model we take the degassing rate uncertainty range from Mills et al. (2021), which is bounded by reconstructions of arc and rift lengths, and by estimates from full-plate models.

5.1.3. Uplift and erosion. Previously, the formulation for the uplift and subsequent erosion of sediments (which affects chemical weathering) was based on a polynomial fit to the depositional record of terrigenous sediments (Ronov 1993, Berner & Kothavala 2001), assuming that erosion rates over the Phanerozoic can be calculated from deposition rates using an erosion-loss relationship (Wold & Hay 1990). The data were normalized to the erosion rates for the Miocene, rather than the Pliocene or Quaternary, in order to avoid the effect of extensive continental glaciation over the past ~5 Myrs on the observed rate (Berner & Kothavala 2001). Erosion was assumed to affect silicate, organic carbon, and sulfide weathering, but not carbonate or sulfate weathering, as it seemed that elevation had little effect on carbonates and sulfates, which can readily dissolve in the subsurface (Berner & Berner 1987; Berner 1991, 2006).

Using the sediment abundance data of Hay et al. (2006), we create minimum and maximum bounds for the Monte Carlo runs by normalizing the data to that of the Pleistocene and Miocene, respectively, and then employ a 100 Myr moving average. Following Li & Elderfield (2013), we include the effect of erosion in the equation for carbonate weathering and assign it a near-linear relationship, while erosion in silicate, organic carbon, and sulfide weathering holds a weaker association.

5.1.4. Effect of O_2 levels on carbon isotope fractionation. As discussed in Section 4, an equation based on plant and algal growth experiments (Berner et al. 2000, Beerling et al. 2002) was used to calculate the changes to photosynthetic $\delta^{13}C$ fractionation at different O_2 levels. The equation required the use of an empirical coefficient, named *J*, which was set to be equal to 4 and seemed to produce $\delta^{13}C$ fractionation in line with that from an even mixture of marine and terrestrial organic matter through time (Hayes et al. 1999, Beerling et al. 2002, Berner 2009). Edwards et al. (2017) used different values for *J* and showed that, in their formulations at least, this parameter had a significant effect on the estimated O_2 levels, while sensitivity testing of this parameter in

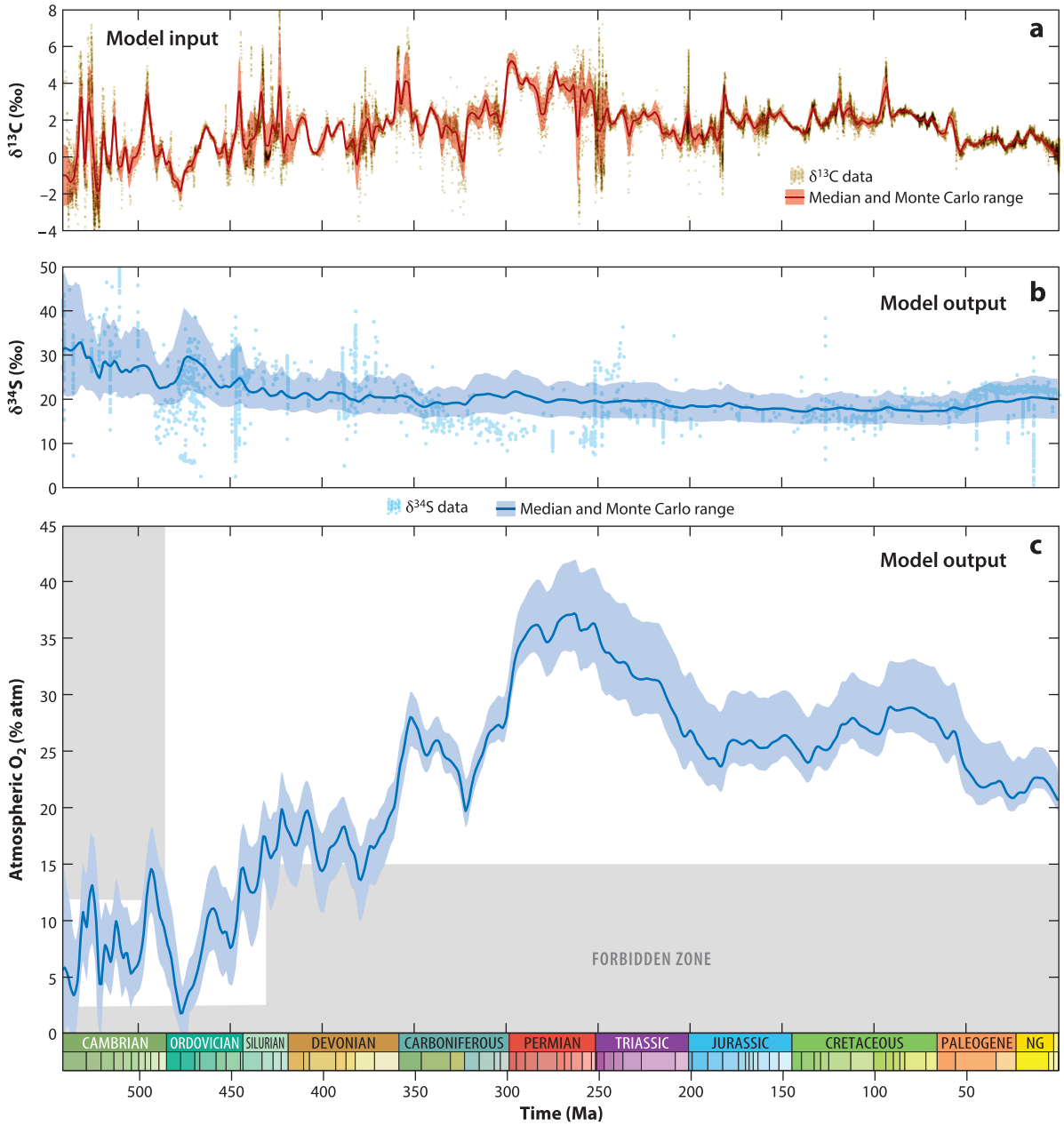

Figure 5

Updated Phanerozoic O_2 predictions from GEOCARBSULFOR. (*a*) Carbonate $\delta^{13}C$ record used as model input, from the GTS2020 (Cramer & Jarvis 2020). (*b*) Sulfate $\delta^{34}S$ record outputted by the model for validation, tested against the compilation of Crockford et al. (2019). (*c*) Predicted Phanerozoic atmospheric O_2 evolution. The central line shows the median, and the blue area shows the full range of the Monte Carlo ensemble. See the text for details of the model and ensemble procedure. The gray areas show the forbidden zone from **Figure 2**. Abbreviation: NG, Neogene.

GEOCARBSULFOR-2018 (Krause et al. 2018) exhibited a far more muted effect, possibly due to other feedbacks in operation. Nevertheless, we include this parameter in the Monte Carlo runs, with minimum and maximum bounds of 2.5 and 7.5, respectively, following Edwards et al. (2017).

5.1.5. Climate sensitivity. The long-term climate sensitivity—the global temperature change expected per CO_2 doubling—is important in estimating the rates of continental weathering through time. In GEOCARBSULF, the climate sensitivity changed through the model run, such that it was approximately 4.32 K per CO_2 doubling during greenhouse periods (e.g., the Cretaceous) and approximately 8.66 K during icehouse periods (e.g., the Carboniferous) (Royer et al. 2014). We instead add climate sensitivity to our Monte Carlo parameters, using the bounds of 4 K and 6 K per CO_2 doubling, which encapsulates the expected Phanerozoic range (e.g., Royer 2016, Mills et al. 2019).

5.1.6. Model stability at low O_2. The GEOCARBSULF and GEOCARBSULFOR-2018 models are highly sensitive to the $\delta^{13}C$ record used as a model input, and very low $\delta^{13}C$ values can result in model failure when more than the entire reservoir of atmospheric and marine O_2 is consumed in a single time step. This problem prevented complete sensitivity analysis being performed by Royer et al. (2014) and Krause et al. (2018). In the updated model we use a logistic function to turn off all O_2-consuming fluxes when oxygen concentration falls below 0.02% atm or 1,000 times less than the present day, which prevents overdepletion of the oxygen reservoir and stops the model crashing during the runs. We still find about 5% of the Monte Carlo runs crash during the model spin-up phase from 570 to 539 Ma where reservoirs initially change size much more rapidly than during the Phanerozoic as the model is adjusting to the starting conditions.

5.1.7. Updated Phanerozoic O_2 reconstruction. New predictions from GEOCARBSULFOR are shown in **Figure 5*b*** and ***c***. The $\delta^{34}S$ record is compared to compiled geological data to ensure that the forwards-calculated sulfur cycle in the model is reasonable. As per Krause et al. (2018), these predictions are in reasonable agreement with the geological record (Crockford et al. 2019). The long-term pattern of Phanerozoic atmospheric O_2 evolution is similar to the previous iteration of the model (Krause et al. 2018), but the new higher fidelity $\delta^{13}C$ record results in more variability in O_2, particularly during the early Paleozoic, with more cyclicity during the Cambrian through to the Devonian. O_2 levels are low during the early Paleozoic and are generally beneath the threshold indicated by widespread ocean anoxia (Canfield 2014, Sperling et al. 2015). The model mean dips slightly below the wildfire minimum during the Devonian, but the uncertainty window remains above the limit. The overall O_2 maximum is shifted back to the Permian, in line with the older GEOCARBSULF models (Berner 2006, 2009). There is also a more pronounced decline in O_2 levels from the end of the Permian across the Triassic.

5.2. A Best Guess for Changes in O_2 Across the Phanerozoic

Figure 6 shows our new combined estimate for Phanerozoic O_2 evolution. The best guess line is the same as that calculated for **Figure 5*c*** from IMB, and the uncertainty window is produced from a smoothed record of the local maximum and minimum from those methods described in Section 4 that do not violate the long-term oxygen constraints. Where parts of their uncertainty windows do violate the constraints, they have been trimmed accordingly. Many of these uncertainty windows overlap with the Monte Carlo uncertainty from the IMB curve and tend to place it close to the middle of the range. Exceptions to this are during the Ordovician, where the direct isotope fractionation method of Edwards et al. (2017) produces significantly higher O_2 (although with a similar trend), and during the Triassic–Jurassic, where the minima from the charcoal inversion and the sedimentary rock mass methods point to lower O_2.

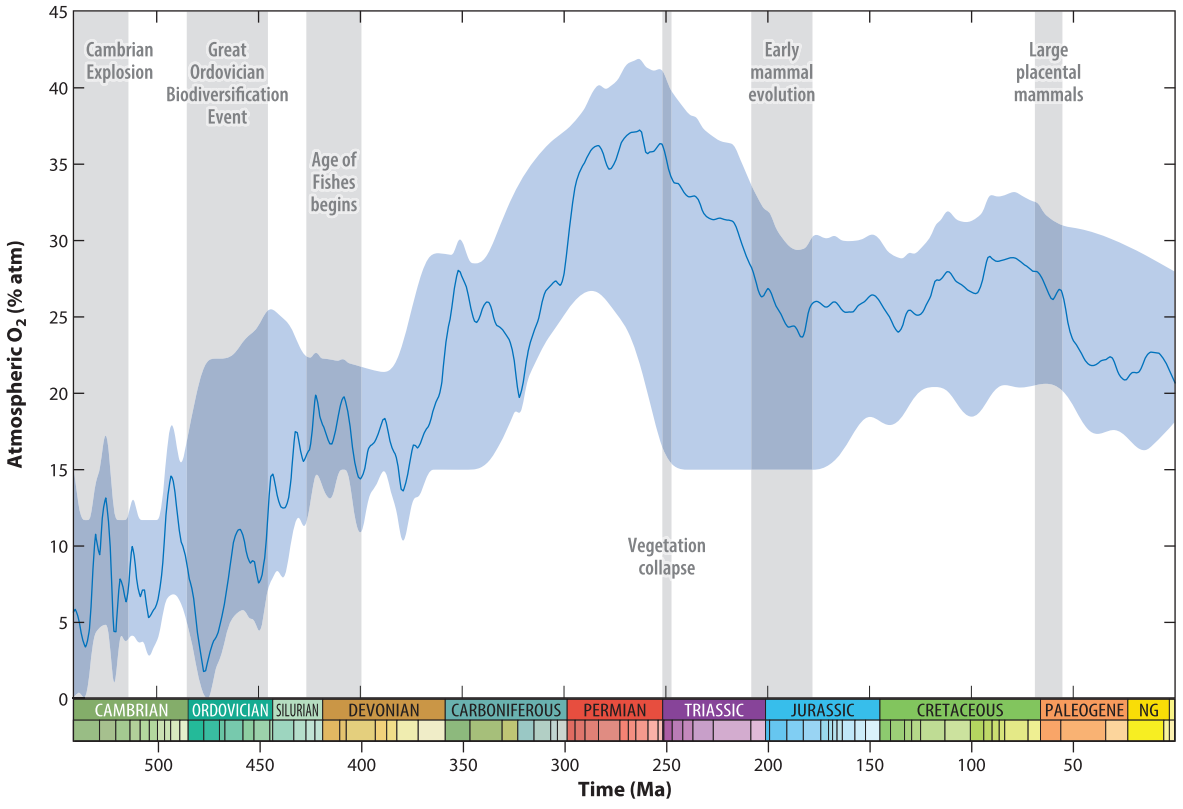

Figure 6

Toward a Phanerozoic O_2 consensus curve. The blue shaded area incorporates all Phanerozoic O_2 estimations from **Figure 3** that do not violate the long-term constraints shown in **Figure 2**. Uncertainty ranges have been trimmed so as to not violate those constraints either. Superimposed on this are the new isotope mass balance O_2 predictions from GEOCARBSULFOR, which also provide the central line. The O_2 variations are compared to key biological events. See the text for further details. The combined O_2 estimate is available to download as a data set from **https://github.com/bjwmills**. Abbreviation: NG, Neogene.

6. HOW DO CHANGES IN O_2 RELATE TO BIOLOGICAL EVENTS?

Alongside our new Phanerozoic O_2 reconstruction in **Figure 6**, we plot a selection of key biotic events, consisting of both evolutionary radiations and crises. The Cambrian Explosion occurred from roughly 541 to 514 Ma (Maloof et al. 2010, Erwin et al. 2011) and saw rapid diversification of all major animal phyla. Our O_2 reconstruction shows substantial variation in oxygen levels during this time, including a series of O_2 pulses during Cambrian stages 2 and 3, which have previously been linked to pulses of biodiversity (He et al. 2019). Without well-defined modeling of the preceding Neoproterozoic Era, we cannot assess whether the Cambrian explosion was triggered by rising O_2 levels, but the periodic changes in biodiversity may well be linked to pulsed atmospheric oxygenation, which would translate to changes in habitable space for animals on the continental shelves. A further expansion of marine animal diversity occurred during the Great Ordovician Biodiversification Event (GOBE), which spans the whole Ordovician period, concentrated in the Middle and Upper Ordovician (Servais & Harper 2018, Edwards 2019). As in the reconstruction of Edwards et al. (2017), we conclude that the Ordovician period was primarily a time of rising oxygen levels, which may have been linked to this event. The Devonian saw several revolutions in the diversity of fish in the oceans, including the evolution of large predatory fish, with their higher

O_2 demands (Dahl et al. 2010, Dahl & Hammarlund 2011). The start of this Devonian "Age of the Fishes" may be extended back into the Silurian, when considering the increase in the biovolume of Chordata (Payne et al. 2009) and a possible evolutionary split between the lungfish and tetrapods (Zhao et al. 2021). It has been estimated that predatory fish need more than 7.4–11.7% O_2 (Dahl & Hammarlund 2011), and our oxygen reconstruction suggests that this threshold was indeed crossed by the late Silurian.

The Permian–Triassic Mass Extinction (PTME) was the most severe of all the Phanerozoic mass extinctions, with 55.7% genus extinction (Erwin 1993, Benton & Twitchett 2003, Bambach 2006). According to our reconstruction, the PTME occurred at a time when atmospheric O_2 levels were the highest they have ever been; considering the devastation and reduction in biomass of terrestrial ecosystems during the event, and into the Middle Triassic (Fielding et al. 2019, Chu et al. 2020, Dal Corso et al. 2020, Xu et al. 2022), the extinction may have been a driver of the subsequent long-term decline in O_2. In our reconstruction, O_2 levels eventually stabilized at around 25% by the Late Triassic, coincident with the evolution of mammals (Sulej et al. 2020). The later evolution of large placental mammals in the early Cenozoic occurs after a long period of gradually rising O_2 levels in our reconstruction (Falkowski et al. 2005), but it is also accompanied by a decline toward present-day levels, making it difficult to link to changes in oxygen concentration.

Overall, pulsed rises in atmospheric oxygen levels appear to be consistent with the Cambrian Explosion, GOBE, and rise of predatory fish, and the general trend throughout the Paleozoic is toward higher and higher atmospheric O_2 levels. This is consistent with a plant evolutionary driver given the successive floral changes occurring during the Paleozoic (Algeo et al. 1995) and the ability of larger and more productive plants to produce more oxygen, although these advances are generally poorly dated, especially in terms of when species rose to ecological dominance. A decline in atmospheric O_2 following the PTME is also consistent with widespread vegetation loss and delayed recovery, which was likely exacerbated by the aridity of the Pangea supercontinent, potentially limiting photosynthetic productivity on land until continental breakup from the Jurassic onward (Chaboureau et al. 2014, Gurung et al. 2022). The drop in O_2 levels between the Late Cretaceous and present day may be related to a decline in global temperatures and runoff over the same timeframe, both of which might be related to decreasing rates of CO_2 degassing (e.g., Brune et al. 2017, Domeier & Torsvik 2017), which would decrease global temperatures and limit the terrestrial biosphere through low CO_2.

7. CONCLUSIONS

New methods for estimating Phanerozoic atmospheric O_2 evolution are widespread, and many older methods are being revised and revisited. At first look, it can be tempting to conclude that no consensus exists on Phanerozoic O_2. We have taken a critical look at the currently available methods and aimed to determine which are the most reliable by comparing them to broadly agreed upon long-term constraints on oxygen concentration. Those methods that currently fail this test are also subject to clear uncertainties in the methodology, which we have highlighted as potential reasons for the divergent results. We have then produced a first attempt at a consensus O_2 curve for the Phanerozoic by bringing together all of the methods that satisfy the long-term constraints. This curve shows that the Cambrian Explosion and GOBE may well be linked to pulses of long-term atmospheric oxygenation, whereas the Devonian "Age of the Fishes" appears to coincide with O_2 levels stabilizing above the threshold which can maintain an oxic ocean interior.

DISCLOSURE STATEMENT

The authors are not aware of any affiliations, memberships, funding, or financial holdings that might be perceived as affecting the objectivity of this review.

ACKNOWLEDGMENTS

B.J.W.M. is funded by the UK Natural Environment Research Council (NE/S009663/1). A.J.K. was funded by the NERC SPHERES Doctoral Training Partnership (NE/L002574/1).

LITERATURE CITED

Ahm A-SC, Bjerrum CJ, Hammarlund EU. 2017. Disentangling the record of diagenesis, local redox conditions, and global seawater chemistry during the latest Ordovician glaciation. *Earth Planet. Sci. Lett.* 459:145–56

Algeo TJ, Berner RA, Maynard JB, Scheckler SE. 1995. Late Devonian Oceanic Anoxic Events and biotic crises: "rooted" in the evolution of vascular land plants? *GSA Today* 5:45–66

Algeo TJ, Ingall E. 2007. Sedimentary C_{org}:P ratios, paleocean ventilation, and Phanerozoic atmospheric pO_2. *Palaeogeogr. Palaeoclim. Palaeoecol.* 256:130–55

Arvidson RS, Mackenzie FT, Guidry MW. 2013. Geologic history of seawater: a MAGic approach to carbon chemistry and ocean ventilation. *Chem. Geol.* 362:287–304

Bambach RK. 2006. Phanerozoic biodiversity mass extinctions. *Annu. Rev. Earth Planet. Sci.* 34:127–55

Beerling DJ, Lake JA, Berner RA, Hickey LJ, Taylor DW, Royer DL. 2002. Carbon isotope evidence implying high O_2/CO_2 ratios in the Permo-Carboniferous atmosphere. *Geochim. Cosmochim. Acta* 66:3757–67

Belcher CM, Collinson ME, Scott AC. 2013. A 450-million-year history of fire. In *Fire Phenomena and the Earth System*, ed. CM Belcher, pp. 229–49. Chichester, UK: Wiley-Blackwell

Belcher CM, McElwain JC. 2008. Limits for combustion in low O_2 redefine paleoatmospheric predictions for the Mesozoic. *Science* 321:1197–200

Benton MJ, Twitchett RJ. 2003. How to kill (almost) all life: the end-Permian extinction event. *Trends Ecol. Evol.* 18:358–65

Bergman NM, Lenton TM, Watson AJ. 2004. COPSE: a new model of biogeochemical cycling over Phanerozoic time. *Am. J. Sci.* 304:397–437

Berner EK, Berner RA. 1987. *The Global Water Cycle: Geochemistry and Environment*. Englewood Cliffs, NJ: Prentice-Hall

Berner RA. 1987. Models for carbon and sulfur cycles and atmospheric oxygen: application to Paleozoic geologic history. *Am. J. Sci.* 287:177–96

Berner RA. 1991. A model for atmospheric CO_2 over Phanerozoic time. *Am. J. Sci.* 291:339–76

Berner RA. 2001. Modeling atmospheric O_2 over Phanerozoic time. *Geochim. Cosmochim. Acta* 65:685–94

Berner RA. 2004. *The Phanerozoic Carbon Cycle: CO_2 and O_2*. Oxford, UK: Oxford Univ. Press

Berner RA. 2006. GEOCARBSULF: a combined model for Phanerozoic atmospheric O_2 and CO_2. *Geochim. Cosmochim. Acta* 70:5653–64

Berner RA. 2009. Phanerozoic atmospheric oxygen: new results using the GEOCARBSULF model. *Am. J. Sci.* 309:603–6

Berner RA, Canfield DE. 1989. A new model for atmospheric oxygen over Phanerozoic time. *Am. J. Sci.* 289:333–61

Berner RA, Kothavala Z. 2001. Geocarb III: a revised model of atmospheric CO_2 over Phanerozoic time. *Am. J. Sci.* 301:182–204

Berner RA, Petsch ST, Lake JA, Beerling DJ, Popp BN, et al. 2000. Isotope fractionation and atmospheric oxygen: implications for Phanerozoic O_2 evolution. *Science* 287:1630–33

Blamey NJF, Brand U. 2019. Atmospheric gas in modern and ancient halite fluid inclusions: a screening protocol. *Gondwana Res.* 69:163–76

Blamey NJF, Brand U, Parnell J, Spear N, Lécuyer C, et al. 2016. Paradigm shift in determining Neoproterozoic atmospheric oxygen. *Geology* 44:651–54

Brand U, Davis AM, Shaver KK, Blamey NJF, Heizler M, Lécuyer C. 2021. Atmospheric oxygen of the Paleozoic. *Earth-Sci. Rev.* 216:103560

Brune S, Williams SE, Müller RD. 2017. Potential links between continental rifting, CO_2 degassing and climate change through time. *Nat. Geosci.* 10:941–46

Budyko MI, Ronov AB, Yanshin AL. 1987. *History of Earth's Atmosphere*. Berlin: Springer-Verlag

Buick R. 2008. When did oxygenic photosynthesis evolve? *Philos. Trans. R. Soc. B* 363:2731–43
Canfield DE. 1998. A new model for Proterozoic ocean chemistry. *Nature* 396:450–53
Canfield DE. 2014. Proterozoic atmospheric oxygen. *Treatise Geochem.* 6:197–216
Canfield DE, Teske A. 1996. Late Proterozoic rise in atmospheric oxygen concentration inferred from phylogenetic and sulphur-isotope studies. *Nature* 382:127–32
Cannell A, Blamey N, Brand U, Escapa I, Large R. 2022. A revised sedimentary pyrite proxy for atmospheric oxygen in the Paleozoic: evaluation for the Silurian-Devonian-Carboniferous period and the relationship of the results to the observed biosphere record. *Earth-Sci. Rev.* 231:104062
Catling DC, Zahnle KJ. 2020. The Archean atmosphere. *Sci. Adv.* 6:eaax1420
Chaboureau AC, Sepulchre P, Donnadieu Y, Franc A. 2014. Tectonic-driven climate change and the diversification of angiosperms. *PNAS* 111:14066–70
Chu D, Grasby SE, Song H, Dal Corso J, Wang Y, et al. 2020. Ecological disturbance in tropical peatlands prior to marine Permian-Triassic mass extinction. *Geology* 48:288–92
Cope MJ, Chaloner WG. 1980. Fossil charcoal as evidence of past atmospheric composition. *Nature* 283:647–49
Cramer BD, Jarvis I. 2020. Carbon isotope stratigraphy. In *Geologic Time Scale 2020*, ed. FM Gradstein, JG Ogg, M Schmitz, G Ogg, pp. 309–43. Amsterdam: Elsevier
Crockford PW, Kunzmann M, Bekker A, Hayles J, Bao H, et al. 2019. Claypool continued: extending the isotopic record of sedimentary sulfate. *Chem. Geol.* 513:200–25
Dahl TW, Hammarlund EU. 2011. Do large predatory fish track ocean oxygenation? *Commun. Integr. Biol.* 4:92–94
Dahl TW, Hammarlund EU, Anbar AD, Bond DPG, Gill BC, et al. 2010. Devonian rise in atmospheric oxygen correlated to the radiations of terrestrial plants and large predatory fish. *PNAS* 107:17911–15
Daines SJ, Mills BJ, Lenton TM. 2017. Atmospheric oxygen regulation at low Proterozoic levels by incomplete oxidative weathering of sedimentary organic carbon. *Nat. Commun.* 8:14379
Dal Corso J, Mills BJW, Chu D, Newton RJ, Mather TA, et al. 2020. Permo–Triassic boundary carbon and mercury cycling linked to terrestrial ecosystem collapse. *Nat. Commun.* 11:2962
Diefendorf AF, Freeman KH, Wing SL. 2012. Distribution and carbon isotope patterns of diterpenoids and triterpenoids in modern temperate C_3 trees and their geochemical significance. *Geochim. Cosmochim. Acta* 85:342–56
Diessel CF. 2010. The stratigraphic distribution of inertinite. *Int. J. Coal Geol.* 81:251–68
Domeier M, Torsvik TH. 2017. Full-plate modelling in pre-Jurassic time. *Geol. Mag.* 156:261–80
Edwards CT. 2019. Links between early Paleozoic oxygenation and the Great Ordovician Biodiversification Event (GOBE): a review. *Palaeoworld* 28:37–50
Edwards CT, Saltzman MR, Royer DL, Fike DA. 2017. Oxygenation as a driver of the Great Ordovician Biodiversification Event. *Nat. Geosci.* 10:925–29
Engebretson DC, Kelley KP, Cashman HJ, Richards MA. 1992. 180 Million years of subduction. *GSA Today* 2:93–100
Erwin DH. 1993. *The Great Paleozoic Crisis. Life and Death in the Permian*. New York: Columbia Univ. Press
Erwin DH, Laflamme M, Tweedt SM, Sperling EA, Pisani D, Peterson KJ. 2011. The Cambrian conundrum: early divergence and later ecological success in the early history of animals. *Science* 334:1091–97
Extier T, Landais A, Bréant C, Prié F, Bazin L, et al. 2018. On the use of $\delta^{18}O_{atm}$ for ice core dating. *Quat. Sci. Rev.* 185:244–57
Falkowski PG, Katz ME, Milligan AJ, Fennel K, Cramer BS, et al. 2005. The rise of oxygen over the past 205 million years and the evolution of large placental mammals. *Science* 309:2202–4
Farquhar J, Bao H, Thiemens M. 2000. Atmospheric influence of Earth's earliest sulphur cycle. *Science* 289:756–58
Fielding CR, Frank TD, McLoughlin S, Vajda V, Mays C, et al. 2019. Age and pattern of the southern high-latitude continental end-Permian extinction constrained by multiproxy analysis. *Nat Commun.* 10:385
Franz HB, Trainer MG, Malespin CA, Mahaffy PR, Atreya SK, et al. 2017. Initial SAM calibration gas experiments on Mars: quadrupole mass spectrometer results and implications. *Planet. Space Sci.* 138:44–54
Gaffin S. 1987. Ridge volume dependence on seafloor generation rate and inversion using long term sealevel change. *Am. J. Sci.* 287:596–611

Garrels RM, Lerman A. 1984. Coupling the sedimentary sulfur and carbon cycles—an improved model. *Am. J. Sci.* 284:989–1007
Garrels RM, Perry EA. 1974. Cycling of C, S and O through geologic time. In *The Sea*, ed. ED Goldberg pp. 303–36. New York: Wiley-Interscience
Glasspool IJ, Gastaldo RA. 2022. Silurian wildfire proxies and atmospheric oxygen. *Geology* 50(9):1048–52
Glasspool IJ, Scott AC. 2010. Phanerozoic concentrations of atmospheric oxygen reconstructed from sedimentary charcoal. *Nat. Geosci.* 3:627–30
Glasspool IJ, Scott AC, Waltham D, Pronina N, Shao L. 2015. The impact of fire on the Late Paleozoic Earth system. *Front. Plant Sci.* 6:756
Gregory BS, Claire MW, Rugheimer S. 2021. Photochemical modelling of atmospheric oxygen levels confirms two stable states. *Earth Planet. Sci. Lett.* 561:116818
Gurung K, Field KJ, Batterman SA, Godderis Y, Donnadieu Y, et al. 2022. Climate windows of opportunity for plant expansion during the Phanerozoic. *Nat. Commun.* 13:4530
Hay WW, Migdisov A, Balukhovsky AN, Wold CN, Flögel S, Söding E. 2006. Evaporites and the salinity of the ocean during the Phanerozoic: implications for climate, ocean circulation and life. *Palaeogeogr. Palaeoclim. Palaeoecol.* 240:3–46
Hayes JM, Strauss H, Kaufman AJ. 1999. The abundance of ^{13}C in marine organic matter and isotopic fractionation in the global biogeochemical cycle of carbon during the past 800 Ma. *Chem. Geol.* 161:103–25
He T, Corso JD, Newton RJ, Wignall PB, Mills BJW, et al. 2020. An enormous sulfur isotope excursion indicates marine anoxia during the end-Triassic mass extinction. *Sci. Adv.* 6:eabb6704
He T, Zhu M, Mills BJW, Wynn PM, Zhuravlev AY, et al. 2019. Possible links between extreme oxygen perturbations and the Cambrian radiation of animals. *Nat. Geosci.* 12:468–74
Hedges JI, Keil RG. 1995. Sedimentary organic matter preservation: an assessment and speculative synthesis. *Mar. Chem.* 49:81–115
Holland HD. 2006. The oxygenation of the atmosphere and oceans. *Philos. Trans. R. Soc. B* 361:903–15
Horscroft JA, Kotwica AO, Laner V, West JA, Hennis PJ, et al. 2017. Metabolic basis to Sherpa altitude adaptation. *PNAS* 114:6382–87
Jørgensen BB, Nelson DC. 2004. Sulfide oxidation in marine sediments: geochemistry meets microbiology. *Geol. Soc. Am. Spec. Pap.* 379:63–81
Kanzaki Y, Kump LR. 2017. Biotic effects on oxygen consumption during weathering: implications for the second rise of oxygen. *Geology* 45:611–14
Krause AJ, Mills BJW, Zhang S, Planavsky NJ, Lenton TM, Poulton SW. 2018. Stepwise oxygenation of the Paleozoic atmosphere. *Nat. Commun.* 9:4081
Kump LR, Fallick AE, Melezhik VA, Strauss H, Lepland A. 2013. The Great Oxidation Event. In *Reading the Archive of Earth's Oxygenation*, ed. VA Melezhik, AR Prave, EJ Hanski, AE Fallick, A Lepland, et al., pp. 1517–33. Berlin: Springer
Large RR, Mukherjee I, Gregory D, Steadman J, Corkrey R, Danyushevsky LV. 2019. Atmosphere oxygen cycling through the Proterozoic and Phanerozoic. *Miner. Depos.* 54:485–506
Lenton TM, Daines SJ, Mills BJW. 2018. COPSE reloaded: an improved model of biogeochemical cycling over Phanerozoic time. *Earth-Sci. Rev.* 178:1–28
Levin L. 2003. Oxygen minimum zone benthos: adaption and community response to hypoxia. *Oceanogr. Mar. Biol.* 41:1–45
Li G, Elderfield H. 2013. Evolution of carbon cycle over the past 100 million years. *Geochim. Cosmochim. Acta* 103:11–25
Liu XM, Kah LC, Knoll AH, Cui H, Wang C, et al. 2021. A persistently low level of atmospheric oxygen in Earth's middle age. *Nat. Commun.* 12:351
Lyons TW, Reinhard CT, Planavsky NJ. 2014. The rise of oxygen in Earth's early ocean and atmosphere. *Nature* 506:307–15
Maloof AC, Porter SM, Moore JL, Dudas FO, Bowring SA, et al. 2010. The earliest Cambrian record of animals and ocean geochemical change. *Geol. Soc. Am. Bull.* 122:1731–74
Mills BJW, Donnadieu Y, Goddéris Y. 2021. Spatial continuous integration of Phanerozoic global biogeochemistry and climate. *Gondwana Res.* 100:73–86

Mills BJW, Krause AJ, Scotese CR, Hill DJ, Shields GA, Lenton TM. 2019. Modelling the long-term carbon cycle, atmospheric CO_2, and Earth surface temperature from late Neoproterozoic to present day. *Gondwana Res.* 67:172–86

Mills BJW, Scotese CR, Walding NG, Shields GA, Lenton TM. 2017. Elevated CO_2 degassing rates prevented the return of Snowball Earth during the Phanerozoic. *Nat. Commun.* 8:1110

Mills DB, Ward LM, Jones C, Sweeten B, Forth M, et al. 2014. Oxygen requirements of the earliest animals. *PNAS* 111:4168–72

Otto-Bliesner BL. 1995. Continental drift, runoff and weathering feedbacks: implications from climate model experiments. *J. Geophys. Res.* 100(D6):11537–48

Payne JL, Boyer AG, Brown JH, Finnegan S, Kowalewski M, et al. 2009. Two-phase increase in the maximum size of life over 3.5 billion years reflects biological innovation and environmental opportunity. *PNAS* 106:24–27

Petit J-R, Raynaud D. 2020. Forty years of ice-core records of CO_2. *Nature* 579:505–6

Pohl A, Ridgwell A, Stockey RG, Thomazo C, Keane A, et al. 2022. Continental configuration controls ocean oxygenation during the Phanerozoic. *Nature* 608:523–27

Poulton SW, Bekker A, Cumming VM, Zerkle AL, Canfield DE, Johnston DT. 2021. A 200-million-year delay in permanent atmospheric oxygenation. *Nature* 592:232–36

Poulton SW, Canfield DE. 2005. Development of a sequential extraction procedure for iron: implications for iron partitioning in continentally derived particulates. *Chem. Geol.* 214:209–21

Pyne SJ, Andrews PL, Laven RD. 1996. *Introduction to Wildland Fire*. New York: Wiley. 2nd ed.

Rasmussen B, Buick R. 1999. Redox state of the Archean atmosphere: evidence from detrital heavy minerals in ca. 3250–2750 Ma sandstones from the Pilbara Craton, Australia. *Geology* 27:115–18

Redfield AC. 1958. The biological control of chemical factors in the environment. *Am. Sci.* 46:205–21

Ronov AB. 1976. Global carbon geochemistry, volcanism, carbonate accumilation, and life. *Geochem. Int.* 13:172–95

Ronov AB. 1993. *Stratisfera—Ili Osadochnaya Obolochka Zemli (Kolichestvennoe Issledovanie)*. Moscow: Nauka (In Russian)

Royer DL. 2016. Climate sensitivity in the geologic past. *Annu. Rev. Earth Planet. Sci.* 44:277–93

Royer DL, Donnadieu Y, Park J, Kowalczyk J, Godderis Y. 2014. Error analysis of CO_2 and O_2 estimates from the long-term geochemical model GEOCARBSULF. *Am. J. Sci.* 314:1259–83

Saltzman MR, Thomas E. 2012. Carbon isotope stratigraphy. In *The Geologic Time Scale 2012*, ed. F Gradstein, J Ogg, M Schmitz, G Ogg, pp. 207–32. Amsterdam: Elsevier

Schachat SR, Labandeira CC, Saltzman MR, Cramer BD, Payne JL, Boyce CK. 2018. Phanerozoic pO_2 and the early evolution of terrestrial animals. *Proc. R. Soc. B* 285:20172631

Scott AC. 1989. Observations on the nature and origin of fusain. *Int. J. Coal Geol.* 12:443–75

Scott AC, Glasspool IJ. 2006. The diversification of Paleozoic fire systems and fluctuations in atmospheric oxygen concentration. *PNAS* 103:10861–65

Scott AC, Glasspool IJ. 2007. Observations and experiments on the origin and formation of inertinite group macerals. *Int. J. Coal Geol.* 70:53–66

Scott AC, Jones TP. 1991. Microscopical observations of recent and fossil charcoal. *Microsc. Anal.* 25:13–15

Servais T, Harper DAT. 2018. The Great Ordovician Biodiversification Event (GOBE): definition, concept and duration. *Lethaia* 51:151–64

Sim MS, Bosak T, Ono S. 2011. Large sulfur isotope fractionation does not require disproportionation. *Science* 333:74–77

Sønderholm F, Bjerrum CJ. 2021. Minimum levels of atmospheric oxygen from fossil tree roots imply new plant–oxygen feedback. *Geobiology* 19:250–60

Sperling EA, Frieder CA, Raman AV, Girguis PR, Levin LA, Knoll AH. 2013. Oxygen, ecology, and the Cambrian radiation of animals. *PNAS* 110:13446–51

Sperling EA, Wolock CJ, Morgan AS, Gill BC, Kunzmann M, et al. 2015. Statistical analysis of iron geochemical data suggests limited late Proterozoic oxygenation. *Nature* 523:451–54

Steadman JA, Large RR, Blamey NJ, Mukherjee I, Corkrey R, et al. 2020. Evidence for elevated and variable atmospheric oxygen in the Precambrian. *Precambrian Res.* 343:105722

Stolper DA, Bender ML, Dreyfus GB, Yan Y, Higgins JA. 2016. A Pleistocene ice core record of atmospheric O_2 concentrations. *Science* 353:1427–30

Sulej T, Krzesinski G, Talanda M, Wolniewicz AS, Blazejowski B, et al. 2020. The earliest-known mammaliaform fossil from Greenland sheds light on origin of mammals. *PNAS* 117:26861–67

Tappert R, McKellar RC, Wolfe AP, Tappert MC, Ortega-Blanco J, Muehlenbachs K. 2013. Stable carbon isotopes of C_3 plant resins and ambers record changes in atmospheric oxygen since the Triassic. *Geochim. Cosmochim. Acta* 121:240–62

Van Cappellen P, Ingall ED. 1994. Benthic phosphorus regeneration, net primary production, and ocean anoxia—a model of the coupled marine biogeochemical cycles of carbon and phosphorus. *Paleoceanography* 9:677–92

Wallace MW, Hood Av, Shuster A, Greig A, Planavsky NJ, Reed CP. 2017. Oxygenation history of the Neoproterozoic to early Phanerozoic and the rise of land plants. *Earth Planet. Sci. Lett.* 466:12–19

Watson AJ, Lenton TM, Mills BJW. 2017. Ocean deoxygenation, the global phosphorus cycle and the possibility of human-caused large-scale ocean anoxia. *Philos. Trans. R. Soc. A* 375:20160318

Wignall PB, Twitchett RJ. 1996. Oceanic anoxia and the end Permian mass extinction. *Science* 272:1155–58

Wildman RA, Hickey LJ, Dickinson MB, Berner RA, Robinson JM, et al. 2004. Burning of forest materials under late Paleozoic high atmospheric oxygen levels. *Geology* 32:457–60

Wold CN, Hay WW. 1990. Estimating ancient sediment fluxes. *Am. J. Sci.* 290:1069–89

Wood R, Liu AG, Bowyer F, Wilby PR, Dunn FS, et al. 2019. Integrated records of environmental change and evolution challenge the Cambrian Explosion. *Nat. Ecol. Evol.* 3:528–38

Wu N, Farquhar J, Strauss H, Kim S-T, Canfield DE. 2010. Evaluating the S-isotope fractionation associated with Phanerozoic pyrite burial. *Geochim. Cosmochim. Acta* 74:2053–71

Xu Z, Hilton J, Yu J, Wignall PB, Yin H, et al. 2022. End Permian to Middle Triassic plant species richness and abundance patterns in South China: coevolution of plants and the environment through the Permian–Triassic transition. *Earth-Sci. Rev.* 232:104136

Yan Y, Brook EJ, Kurbatov AV, Severinghaus JP, Higgins JA. 2019. Ice core evidence for atmospheric oxygen decline since the Mid-Pleistocene transition. *Sci. Adv.* 7:eabj9341

Zhang S, Planavsky NJ, Krause AJ, Bolton EW, Mills BJW. 2018. Model based Paleozoic atmospheric oxygen estimates: a recent visit to GEOCARBSULF. *Am. J. Sci.* 318:557–89

Zhao W, Zhang X, Jia G, Shen Y, Zhu M. 2021. The Silurian-Devonian boundary in East Yunnan (South China) and the minimum constraint for the lungfish-tetrapod split. *Sci. China Earth Sci.* 64:1784–97